Evando S. Araújo[1, 2], Marcio Luis F. Nascimento[2], Helinando P. de Oliveira[1]

Electrospinning of Polymeric Fibres: an Unconventional View on the Influence of Surface Tension on Fibre Diameter

DOI: 10.5604/12303666.1172083

[1]Institute of Research in Materials Science, Federal University of São Francisco Valley, 48920-310, Juazeiro, BA, Brazil.
E-mail: helinando.oliveira@univasf.edu.br

[2]Graduate Program in Industrial Engineering, Polytechnic School, Federal University of Bahia, 40210-630, Salvador, BA, Brazil.

Abstract
The production of regular and bead-free electrospun polymeric fibres requires an adequate combination of different parameters applied in the experimental setup viz. voltage for electrodeposition, viscosity of the solution, density of the polymeric support, the distance between electrodes and the geometry of the spinneret. Determination of the physical balance of forces on the droplet during fibre production was explored and provides relevant theoretical information about the surface tension and radius of polymeric fibres. Based on these predictions, we prepared polymeric electropun fibres of poly (vinyl alcohol), poly (vinyl pyrrolidone) and Eudragit® L100 in order to analyse non-conventional physical properties of experimental systems such as droplet stiffness and their influence on the diameter of resulting fibres.

Key words: *electrospinning, polymeric fibres, Taylor´s cone, surfactant, surface tension.*

Introduction

The production of fibrilar structures represents an important strategy for the development of more efficient 1-D composites, with potential application as photocatalysts [1, 2], solar cell devices [3 - 5], artificial muscles and tissue [6 - 9], bactericidal agent [10, 11], drug delivery systems [12, 13] and so on [14 - 16]. The development of 1-D structures introduces an additional advantage for improvement in the typical surface to volume ratio.

Electrospinning is a simple and low cost technique based on the use of charged droplets that draw very fine (typically on a micro/nano scale) fibres from a liquid. The development of this technique has a rich and long history, including centuries of discoveries and applications [17]. Firstly it was patented by John F. Cooley in 1900 [18], improved by Anton Formhals (1934) [19] and recently explored by Doshi and Reneker [20] in the production of nanofibres of different polymeric templates (even large and complex molecules) such as poly(vinyl pyrrolidone) - PVP [21], poly(latic acid) [22] and poly(vinyl alcohol) - PVA [23]. Particularly PVA and PVP are promising candidates for different applications due to their unique properties such as swelling in aqueous solution. On the other hand, anionic copolymers of methacrylic acid and methyl methacrylate (Eudragit® L100) developed by Evonik Industries have been extensively explored as enteric polymers [24, 25], in which the solubility depends on the pH of the media. In this direction, the production of homogeneous fibres of Eudragit® L100 for controlled release of drugs represents a new and promising area to be explored.

A theoretical study of electrospinning processes was reported by Zeleny [26 - 28] in the form of an analysis of electrical discharge from liquid points. These studies were continued by Taylor [29], Drozin [30], Baumgarten [31] and Doshi & Reneker [20].

Recently theoretical studies on electrodeposition have been carried out by different groups. Gañán [32, 33] proposed a 1D model of the equilibrium of an electrified jet applied in the transition between the Taylor´s cone and linear segment of the fluidic jet under electrical forces. Hohman *et al*. [34, 35] studied the stability of fluidic jets under the influence of an electrical field and concluded that instability in the scattering zone is a consequence of interaction between the surface charge density of the jets and the external electric field. In addition, the effect of temperature on the description of the movement of the fluid was considered in [36] from an adaptation of Maxwell's and Navier-Stokes equations. Reneker *et al*. [37-42] proposed an interesting model which provides a complete description of four different regions during the electrospinning process (illustrated in the ***Figure 1***).

Based on these studies, Reneker & Yarin [43] reported that polymeric chain relaxation affects the stretching in the linear segment region, where a flux with a stretching rate of 20 s^{-1} is controlled

by the effects of the electric potential and stretching tension.

In spite of a wide number of studies on electrospinning, a generalisation of the influence of surface tension (controlled by additives such as surfactants) on the overall processes of electrodeposition remains an important topic for analysis and application in industry.

In this direction, we studied fundamental physical equations applied to a droplet under an intense electric field (during the electrospinning process), which allows the development of a simple mathematical function that relates the diameter of fibre with surface tension to the droplet. The resulting relationship was checked for three different experimental systems *viz.* PVA, PVP and Eudragit® L100.

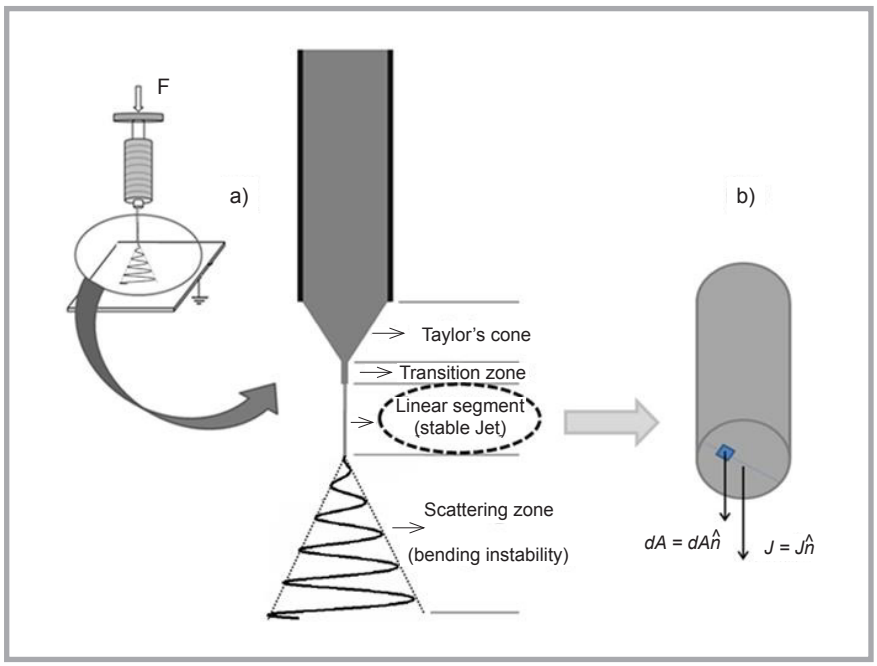

Figure 1. *a) Schematic representation of different regions during electrospinning procedure, b) detail of linear segment for fibre formation.*

Experimental

Eudragit® L100 (EDGT) (Evonik Industries, Germany), poly(vinyl alcohol) (Aldrich, USA), poly(vinyl pyrrolidone) (Aldrich, USA) and non-ionic surfactant triton X-100 (TX-100) (Aldrich, USA) were used as received.. PVA hydrogel was prepared from an inclusion of 4 g of PVA in 50 ml of milli-*Q* water in a thermal bath for 3 hours at 80 °C until complete dispersion of the polymer. An alcoholic solution of polyvinyl pyrrolidone (PVP) was prepared from a mixture of 1.3 g of PVP in 2.53 ml of ethyl alcohol at 25 °C until complete dispersion of the polymer.

1.4 g of EDGT was dispersed in 7 ml of ethylic alcohol. The resulting solution was vigorously stirred for 10 minutes until complete dispersion of the polymer. Electrospun PVA nanofibres were prepared at a relative concentration of 0, 1, 2, 5, 8 and 11% of TX-100 (in wt), while fibres of EDGT and PVP nanofibres were prepared using 0, 2, 5, 8, 11 and 15% of TX-100 (in wt).

The surface tension was measured at 25 °C using a standard drop-weight method [44,45]. A variable amount of surfactant (TX-100) was added to the hydrogel solution, and maintained under fixed pressure in a flux of 166 µl min^{-1} in the absence of an external electric field (this parameter represents the optimised condition established in our experimental setup, allowing the best configuration for continuous fibre production) [46].

The capillary is a metal cylinder compartment with a uniform diameter of 0.7 mm with a planar interface (the orifice at the extremity of the spinneret is cut in a parallel plane with a grounded target - as schematically drawn in ***Figure 1***).

An electrical excitation from a high voltage source (15 kV) is established between the needle and grounded target (separated by 10 cm). As a result, the sample holder (a metallic flat surface attached to the surface of a grounded target plane) collects the ejected fibres, carried out for 5 minutes.

Statistical data treatment was performed using the software Minitab 14 (statistics package) and ImageJ (a public-domain image processing and analysis program developed at the U.S. National Institute of Health (NIH)) [47 - 50], and SEM images were acquired using microscopy - Hitachi TM1000 (Japan).

For data analysis, we examined three independent microscopies of resulting fibres for each relative concentration of PVA/TX-100, EDGT/TX-100 and PVP/TX-100. We considered images in which at least 30 different fibres were registered since DeHoff and Rhines [51] established that normal distribution is expected if at least 30 individual measurements are available, as chosen in the present work.

From these images we determined the average fibre diameter ($\bar{d}$) and corresponding standard deviation ($s_{\bar{d}}$) for each of the 9 samples. The Kolmogorov-Smirnov (*KS*) hypothesis [52] with a significance (α) of 0.05 was estimated in order to identify the normal diameter distribution.

The media of fibre diameter ($d = 2r$) for each concentration of TX-100 was estimated from average data ($\bar{d}$, $s_{\bar{d}}$ and n), and given by value intervals $(\bar{d} - t_{(\frac{\alpha}{2},n-1)}\frac{s_{\bar{d}}}{\sqrt{n}};\ \ \bar{d} + t_{(\frac{\alpha}{2},n-1)}\frac{s_{\bar{d}}}{\sqrt{n}})$ with *Student's t distribution* ($\alpha = 0.05$ and $n - 1$ degrees of freedom) using a 95% confidence interval [53, 54].

Results and discussion

Theoretical background

The resulting forces on the surface of the droplet during polymeric ejection are the electrical force, weight and force due to the surface tension contribution, according ***Equation 1***:

$$\overrightarrow{(F_E} + \vec{P}) - \overrightarrow{F_S} = m\vec{a} \qquad (1)$$

$\overrightarrow{F_E}$ is the electrical force, $\overrightarrow{F_S}$ the surface force on the droplet, given by $F_s = 2\pi R\gamma$, (R is the radius of the droplet and γ the surface tension of polymeric solution at the interface of air/end of needle); m represents the mass of the droplet ($P = mg$), P the corresponding weight, g the acceleration of gravity, and $\vec{a}$ is

the resulting acceleration of the jet in the direction to the grounded target. The direct relationship between the current and the droplet radius is given by:

$$I = JA = \rho\mu\pi r^2 \quad (2)$$

J is the current density, A the cross section area of the ejected fibre ($A = \pi r^2$) (as illustrated in ***Figure 1***), r the radius of resulting fibre, ρ the charge density, and μ the velocity of ejected fibre in the direction of the target. Based on ***Equation 2***, it is possible to write parameter r in terms of current, according ***Equation 3***:

$$r = \sqrt{\frac{I}{\rho\mu\pi}} \quad (3)$$

By application of the first derivative in terms of time in ***Equation 3***:

$$\frac{dr}{dt} = -\frac{1}{2}\sqrt{\frac{I}{\rho\pi}}\mu^{-3/2}\frac{d\mu}{dt} = \\ = -\frac{1}{2}\sqrt{\frac{I}{\rho\pi}}\mu^{-3/2}a \quad (4)$$

According ***Equation 3***, we can use that r is proportional to $\mu^{-1/2}$. As a consequence,

$$\frac{dr}{r^3} \approx -\frac{1}{2}\sqrt{\frac{I}{\rho\pi}}a\,dt \quad (5)$$

After the integration of ***Equation 5***:

$$r^{-2} \approx \sqrt{\frac{I}{\rho\pi}}a\,t \quad (6)$$

According ***Equation 6***, we can write the acceleration in terms of the radius of the droplet. After substitution in ***Equation 1***:

$$r \approx \left(\frac{\rho\pi}{I}\right)\left[\frac{m}{(F_E + mg - F_S)t}\right]^{1/2} \quad (7),$$

In terms of surface tension ($\gamma = F_S/2\pi R$), we can rewrite ***Equation 7*** as:

$$r \approx \left(\frac{\rho^2\pi m}{2RI^2t}\right)^{1/2}\left(\frac{1}{\frac{(F_E + mg)}{2\pi R} - \gamma}\right)^{1/2} \quad (8)$$

The overall dependence of diameter d ($d = 2r$) of the resulting fibre versus the surface tension can be described by a typical function

$$d(\gamma) = \frac{k}{\sqrt{k_1 - \gamma}} \quad (9)$$

with $k \approx \sqrt{\frac{\rho^2\pi m}{2RI^2t}}$ and $k_1 = \frac{F_E + mg}{2\pi R}$.

k_1 can be physically interpreted as a characteristic constant of the droplet stiffness given in N/m (corresponding physical unity). High values of k_1 are assigned to materials in which a high external electric field affects minimally the structure of the droplet during electrospinning, allowing the uniform ejection of fibres with a sharp distribution of the diameter. In this direction, k_1 can be used as an indication of the degree of elasticity of the droplet as a response to the external electric field.

Application of a physical model to experimental electrospun fibres' results

The experimental data relationship between the surface tension and fibre diameter for electrospun fibres of PVA is provided by the images in ***Figure 2***. As we can see, beads are dispersed in the nanofibres of neat PVA. These defects are provoked by fast droplet deposition on the target. Beads are minimised in the resulting net with adequate control of surface tension on the droplet. Recently we have published a study in which TX-100 is applied in the minimisation of beads on a polymeric net of PVA [46]. Results indicated that the number of beads is strongly affected by a reduction in the surface tension of the polymeric solution due to the progressive inclusion of TX-100. Associated with the production of regular fibres (low concentration of beads), surfactant addition strongly affects the average diameter of fibres, providing variation from 994 nm to 278 nm.

The influence of TX-100 on the production of PVP fibres (data and images shown in ***Figure 3***, see page 26) indicates a reduction in the diameter of electrospun fibres from 10 μm to 2 μm. A negligible concentration of beads is verified in the complete range of samples analysed.

The dependence of the diameter of fibres of EDGT with TX-100 concentration is shown in ***Figure 4***, see page 27, in which it is possible to verify a reduction in the diameter of fibres from 8.62 μm to 3.16 μm.

Complementary statistical data *viz.* the *p*-value of the Kolmogorov-Smirnov normality test [52] and the confidence interval for the average diameters (d) of samples PVA, PVP and EDGT are summarised in ***Table 1***.

If organized in the same plot, corresponding data of the resulting PVA fibre diameter versus surface tension (shown in ***Figure 5***, see page 28) follow ***Equation 9***. Corresponding fitting data values are indicated in the inset of ***Figure 5***. As we can see, fitting parameters showed that the droplet stiffness of PVA (parameter k_1 in the ***Equation 9***) is 81.8 N/m.

The relationship between the experimental data and the best parameters for the fitting of fibres based on PVP are shown in *t **Figure 6***, see page 28. The value of k_1 for PVP is 76.4 N/m.

The dependence of the diameter of fibres with a surface tension of Eudragit® L100 - based fibres (***Figure 7***, see page 28) gives a value of 40 N/m to k_1.

Overall results indicate that progressive inclusion of the surfactant on the polymeric solution reduces surface tension on the droplet. As a result, the reduction in the surface tension strongly affects the rate of deposition due to the changes in the balance of forces during electrodeposition. A relative concentration of 11% of TX-100 reduces by 70% the diameter of fibres of PVA, while 15% of TX-100 reduces by 80% that of resulting fibres of PVP and 63% of that of EDGT fibres. Qualitative data are in agreement

Table 1. *Statistical data: p-value of Kolmogorov-Smirnov normality test and confidence interval (d_{min}; d_{max}) for diameter (d) of PVA, PVP and EDGT fibres as a function of TX-100 concentration: * p-value > 0.05: normal distribution.*

TX-100, wt %	PVA fibres		PVP fibres		Eudragit®L100 fibres	
	p-value	d_{min}; d_{max}, nm	*p-value*	d_{min}; d_{max}, μm	*p-value*	d_{min}; d_{max}, μm
0	< 0.01	915.70; 1072.51	> 0.15*	10.15; 11.26	> 0.15*	8.05; 9.19
1		632.80; 695.40	-	-	-	-
2	> 0.15*	453.23; 525.77	> 0.15*	6.52; 7.36		4.96; 5.64
5		375.43; 444.97	0.121*	4.16; 4.76		3.29; 3.92
8	0.113*	295.45; 333.35	> 0.15*	2.90; 3.41	> 0.15*	3.29; 3.92
11	> 0.15*	261.90; 295.90	< 0.01	1.97; 2.65		3.09; 3.65
15	-	-	0.095*	1.92; 2.25		2.89; 3.43

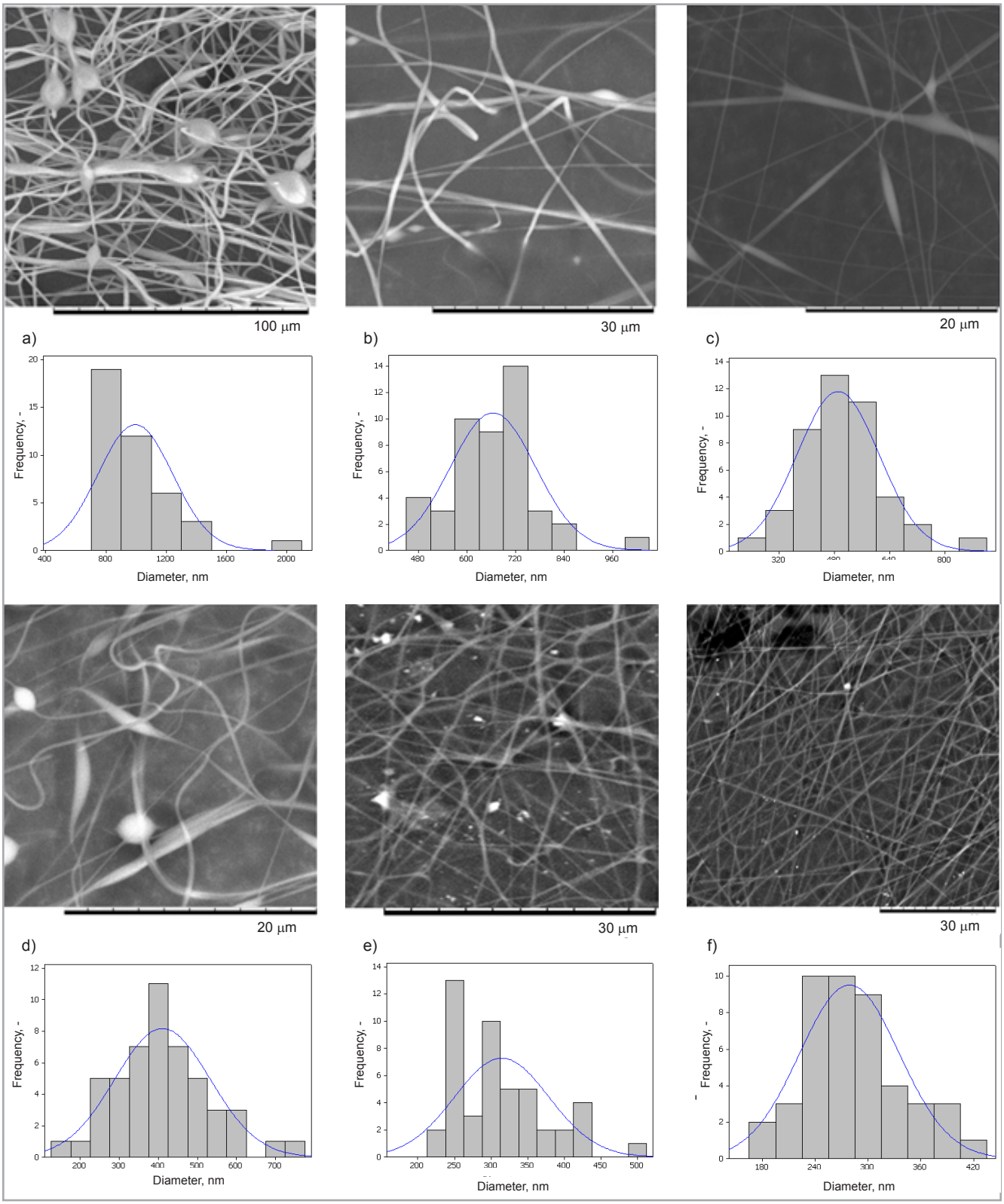

Figure 2. *Distribution of PVA fibre diameters (d) at different relative concentrations of TX-100; a) 0%, b) 1% c) 2%, d) 5%, e) 8%, f) 11%.*

with results reported by Ramakrishna *et al*. [55] which indicated that the diameter *d* of fibres is proportional to that of the droplet at the tip of the needle (2*R*).

As regards the surface tension affecting the size of the droplet at the tip of the needle, we can verify that the relative concentration of surfactant affects ***Equation 1***: the reduction in the diameter of the droplet decreases the weight and, consequently, the density of the charge at the extremity of the droplet. The electrospinning process is established with the ejection of fibres at a specific rate and instability induced by a regular flux of beads is minimised. As a result, a reduction in the diameter of fibres is accomplished by the minimal dispersion of beads in the resulting net.

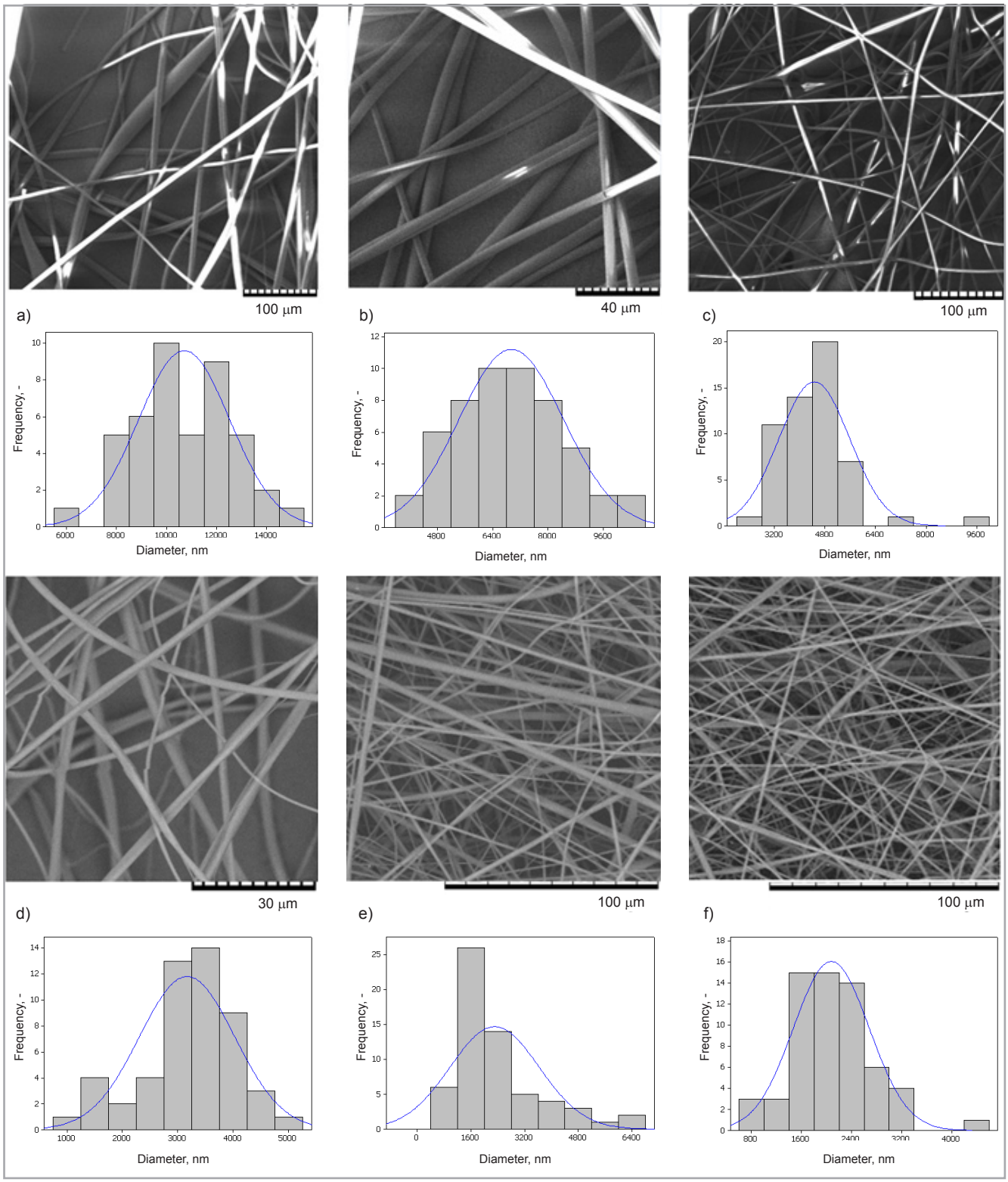

Figure 3. *Distribution of PVP fibre diameters (d) at different relative concentrations of TX-100; a) 0%, b) 2% c) 5%, d) 8%, e) 11%, f) 15%.*

In this direction, the use of parameter K_1 in comparison with measurement of the diameter of the droplet introduces advantages for quantification of the influence of the size and stiffness of the droplet on the diameter of resulting fibres.

By comparison of values, we can verify that $k_{1PVA} > k_{1PVP} > k_{1EDGT}$, which is in agreement with the inverse order of the diameter of resulting fibres: $d_{PVA} < d_{PVP} < d_{EDGT}$; is an indication that elevation in the mechanical resistance of the droplet to external excitation contributes to a reduction in the diameter of resulting fibres.

The droplet's stiffness can be explored as an important parameter applied in the estimation of the potential of polymeric templates for application in fibre production with minimal dispersion and

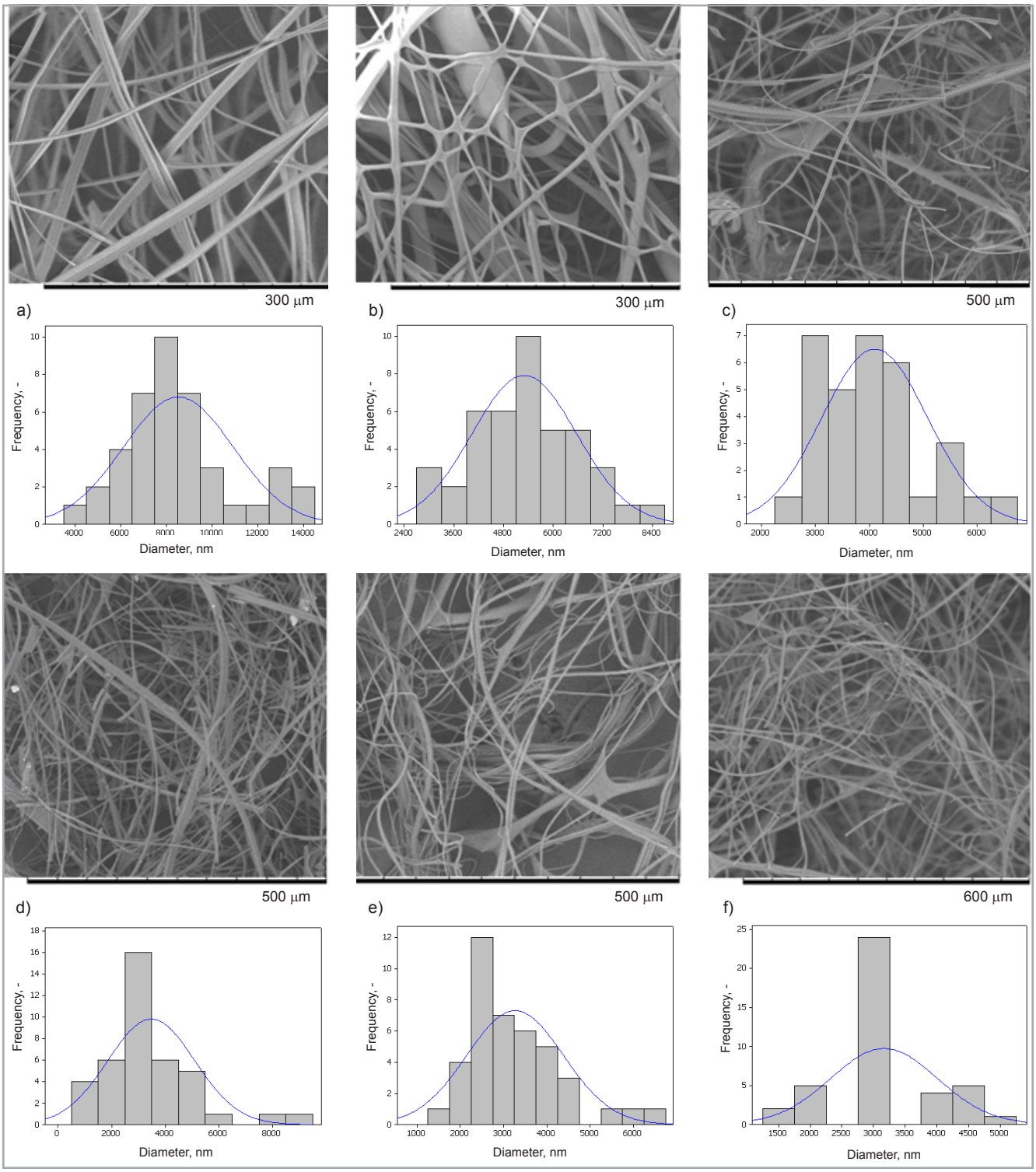

Figure 4. *Distribution of Eduragit® L100 fibre diameters (d) at different relative concentrations of TX-100.; a) 0%, b) 2% c) 5%, d) 8%, e) 11%, f) 15%.*

progressive reduction in the diameter of ejected fibres.

Conclusions

The production of electrospun fibres with a controlled diameter and minimal distribution of imperfections (beads) presents a strong dependence with surface tension on the droplet (disposed at the tip of needle). A first principle model that describes the resulting force on the needle was explored in order to predict the influence of the surface tension of the droplet on the diameter of resulting fibres, and reasonable agreement with experimental data was obtained.

According to the model, droplet stiffness (parameter k_1) – as a substitution for conventional measurement of the droplet diameter - can be conveniently explored as a direct measurement of the spinnability potential of specific hydrogel. It represents an intrinsic property of material which reflects the instability of the droplet under the influence of an external electric field.

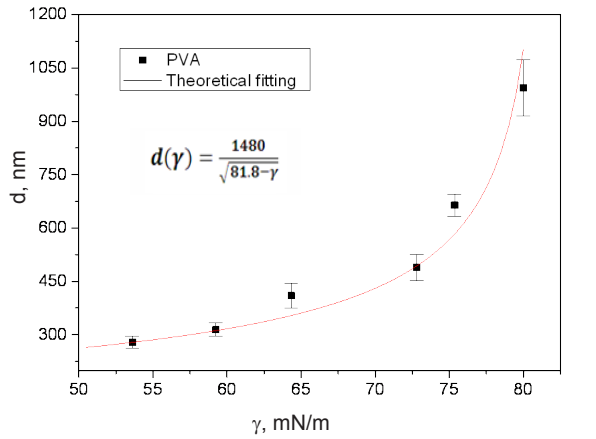

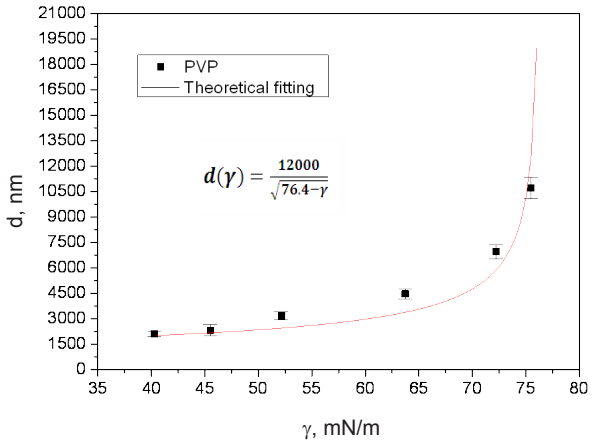

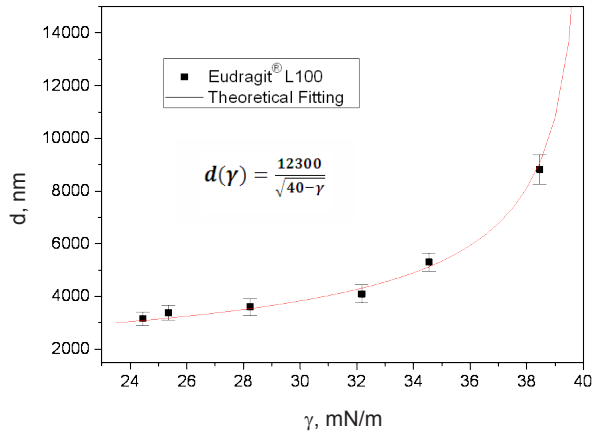

Figure 5. *Dependence of the diameter of PVA fibres (d) versus surface tension (γ).*

Figure 6. *Diameter of PVP fibres (d) versus surface tension (γ).*

Figure 7. *Diameter of Eduragit® L100 fibres (d) versus surface tension (γ).*

Acknowledgments

The authors gratefully acknowledge financial support from Brazilian Funding Agencies FACEPE, CNPq, CAPES and FAPESB.

References

1. Ma D, Xin Y, Gao M, Wu J. Fabrication and photocatalytic properties of cationic and anionic S-doped TiO2 nanofibers by electrospinning. *Appl. Catal. b-Environ.* 2014; 147: 49-57.
2. Hassan MS, Amna T, Khil MS. Synthesis of high aspect ratio CdTiO3 nanofibers via electrospinning: characterization and photocatalytic activity. *Ceram. Int.* 2014; 40: 423-427.
3. Hieu NT, Baik SJ, Chung OH, Park JS. Fabrication and characterization of electrospun carbon nanotubes/titanium dioxide nanofibers used in anodes of dye-sensitized solar cells. *Synth. Met.* 2014; 193: 125-131.
4. Jin EM, Park JY, Zhao XG, Lee IH, Jeong SM, Gu HB. Photovoltaic properties of TiO2–ZrO2 fiber composite electrodes for dye-sensitized solar cells. *Mater. Lett.* 2014; 126: 281-284.
5. Yang S, Nair AS, Ramakrishna S. Conversion efficiency enhancement of CdS quantum dot-sensitized electrospun nanostructured TiO2 solar cells by organic dipole treatment. *Mater. Lett.* 2014; 116: 345-348.
6. Dargaville BL, Vaquette C, Rasoul F, Cooper-White JJ, Campbell JH, Whittaker AK. Electrospinning and crosslinking of low-molecular-weight poly(trimethylene carbonate-co-(L)-lactide) as an elastomeric scaffold for vascular engineering. *Acta Biomater.* 2013; 9: 6885-6897.
7. Hong CH, Ki SJ, Jeon JH, Che HL, Park IK, Kee CD, Oh IK. Electroactive bio-composite actuators based on cellulose acetate nanofibers with specially chopped polyaniline nanoparticles through electrospinning. *Compos Sci Technol* 2013; 87:135-141.
8. Ha YM, Amna T, Kim MH, Kim HC, Hassan MS, and Khil MS. Novel silicificated PVAc/POSS composite nanofibrous mat via facile electrospinning technique: potential scaffold for hard tissue engineering. *Colloid Surface B* 2013; 102: 795-802.
9. Mouthuy PA, Crossley A, Ye H. Fabrication of calcium phosphate fibres through electrospinning and sintering of hydroxyapatite nanoparticles. *Mater. Lett.* 2013; 106: 145-150.
10. Celebioglu A, Aytac Z, Umu OCO, Dana A, Tekinay T, Uyar T. One-step Synthesis of size-tunable Ag nanoparticles incorporated in electrospun PVA/cyclodextrin nanofibers. *Carbohyd. Poly.* 2014; 99: 808-816.
11. Pant B, Pant HR, Barakat NAM, Park M, Jeon K, Choi Y, Kim HY. Carbon nanofibers decorated with binary semiconductor (TiO_2/ZnO) nanocomposites for the effective removal of organic pollutants and the enhancement of antibacterial activities. *Ceram. Int.* 2013; 39: 7029-7035.
12. Sill TJ, von Recum HA. Electrospinning: applications in drug delivery and tissue engineering. *Biomaterials* 2008; 29: 1989-2006.
13. Hu X, Liu S, Zhou G, Huang Y, Xie Z, Jing X. Electrospinning of polymeric nanofibers for drug delivery applications. *J. Control. Release* 2014; 185: 12-21.
14. Sun B, Long YZ, Zhang HD, Li MM, Duvail JL, Jiang XY, Yin HL. Advances in three-dimensional nanofibrous macrostructures via electrospinning. *Prog. Polym. Sci.* 2014; 39: 862-890.
15. Agarwal S, Greiner A, Wendorff JH. Functional materials by electrospinning of polymers. *Prog. Polym. Sci.* 2013; 38(6): 963-991.
16. Bhardwaj N, Kundu SC. Electrospinning: a fascinating fiber fabrication technique. *Biotechnol. Adv.* 2010; 28: 325-347.
17. Tucker N, Stanger J, Staiger MP, Razzaq H, Hofman K. The history of the science and technology of electrospinning from 1600 to 1995. *J. Eng. Fiber. Fabr.* 2012; 7: 63-73.
18. Cooley JF. Improved methods of and apparatus for electrically separating the relatively volatile liquid component from the component of relatively fixed substances of composite fluids. Patent 06385, GB, 1900.

19. Formhals A. Process and apparatus for preparing artificial threads. Patent 1975504, USA, 1934.
20. Doshi J, Reneker DH. Electrospinning process and application of electrospun fibers. *J. Electrostat.* 1995; 35: 151-160.
21. McCann JT, Li D, Xia YN. Electrospinning of nanofibers with core-sheath, hollow, or porous structures. *J. Mater. Chem.* 2005; 15: 735-738.
22. Picciani PHS, Soares BG, Medeiros ES, Souza Junior FG, Wood DF, Orts WJ, Mattoso LHC. Electrospinning of Polyaniline/Poly(Lactic Acid) Ultrathin fibers: process and statistical modeling using a non-gaussian approach. *Macromol. Theor. Simul.* 2009; 18: 528-536.
23. Costa RGF, Ribeiro C, Mattoso LHC. Morphological and photocatalytic properties of PVA/TiO2 nanocomposite fibers produced by electrospinning. *J. Nanosci. Nanotechn.* 2010; 10: 5144-5152.
24. de Oliveira HP, Albuquerque Jr JJF, Nogueiras C, Rieumont J. Physical chemistry behavior of enteric polymer in drug release systems. *Int. J. Pharm.* 2009; 366: 185-189.
25. de Oliveira HP, Tavares GF, Nogueiras C, Rieumont J. Physico-chemical analysis of metronidazole encapsulation processes in Eudragit copolymers and their blending with amphiphilic block copolymers. *Int. J. Pharm.* 2009; 380: 55-61.
26. Zeleny J. The electrical discharge from liquid points, and a hydrostatic method of measuring the electric intensity at their surfaces. *Phys. Rev.* 1914; 3: 69-91.
27. Zeleny J. Instability of electrified liquid surfaces. *Phys. Rev.* 1917; 10:1-6.
28. Zeleny J. Electrical discharges from pointed conductors. *Phys. Rev.*1920; 16: 102-125.
29. Taylor G. Electrically driven jets. *Proc. R. Soc. Lond. A.* 1969; 313: 453-475.
30. Drozin VG. The electrical dispersion of liquids as aerosols. *J. Colloid. Sci.* 1955; 10: 158-164.
31. Baumgarten PK. Electrostatic spinning of acrylic microfibers. *J. Colloid. Interf. Sci.* 1971; 36: 71-79.
32. Gañán AM. Cone-Jet Analytical Extension of Taylor's Electrostatic Solution and the Asymptotic Universal Scaling Laws in Electrospraying. *Phys. Rev. Lett.* 1997; 79: 217-220.
33. Gañán AM. The surface charge in electrospraying: its nature and its universalscaling laws. *J. Aerosol. Sci.* 1999; 30: 863-872.
34. Hohman MM, Shin YM, Rutledge GC, Brenner MP. Electrospinning and electrically forced jets. I. Stability theory. *Phys. Fluids.* 2001; 13: 2201-2220.
35. Hohman MM, Shin YM, Rutledge GC, Brenner MP. Electrospinning and electrically forced jets. II. Applications. *Phys Fluids* 2001; 13: 2221-2236.
36. Wan YQ, Guo Q, Pan N. Thermo-electro-hydrodynamic model for electrospinning process. *Int. J. Nonlinear Sci. Num. Simul.* 2004; 5: 5-8.
37. Yarin AL, Koombhongse S, Reneker DH. Taylor cone and jetting from liquid droplets in electrospinning of nanofibers. *J. Appl. Phys.* 2001; 90: 4836-4846.
38. Yarin AL, Koombhongse S, Reneker DH. Bending instability in electrospinning of nanofibers. *J. Appl. Phys.* 2001; 89: 3018-3026.
39. Yarin AL, Chase GG, Liu W, Doiphode SV, Reneker DH. Liquid drop growth on a fiber. *Aiche. J.* 2006; 52: 217-227.
40. Han T, Reneker DH, Yarin AL. Pendulum-like motion of straight electrified jets. *Polymer* 2008; 49: 2160-2169.
41. Han T, Yarin AL, Reneker DH. Viscoelastic electrospinning jets: initial stresses and elongation rheometry. *Polymer* 2008;49:1651-1658.
42. Reneker DH, Yarin AL, Fong H, Koombhongse S. Bending instability of electrically charged liquid jets of polymer solutions in electrospinning. *J. Appl. Phys.* 2000; 87: 4531-4547.
43. Reneker DH, Yarin AL. Electrospinning jets and polymer nanofibers. *Polymer* 2008; 49: 2387-2425.
44. Gans DM, Harkins WD. The drop weight method for the determination of surface tension. The effect of an inclination of the tip upon the drop weight. *J. Am. Chem. Soc.* 1930; 52(6): 2287–228.
45. Bailey KC. Determination of Surface Tension by the Drop-Weight Method. *Nature* 1936; 137: 323-323.
46. Araújo ES, Nascimento MLF, de Oliveira HP. Influence of Triton X-100 on PVA fibres production by electrospinning technique. *Fibres & Textiles in Eastern Europe* 2013; 21: 39-43.
47. Collins TJ. ImageJ for microscopy. *Biotechniques* 2007; 43: 25-30.
48. Barboriak DP, Padua AO, York GE, MacFall JR. Creation of DICOM-aware applications using ImageJ. *J. Digit. Imaging.* 2005;18: 91-99.
49. Rajwa B, Mcnally HA, Varadharajan P, Sturgis J, Robinson JP. AFM/CLSM data visualization and comparison using an open-source toolkit. *Microsc. Res. Techniq.* 2004; 64: 176-184.
50. Eliceiri KW, Rueden C. Tools for visualizing multidimensional images from living specimens. *Photochem. Photobiol.* 2005; 81: 1116-1122.
51. DeHoff RT, Rhines FN (Eds.). *Quantitative Microscopy*. New York: McGraw-Hill, 1968.
52. Kolmogorov AN. Sulla determinazione empirica di una legge di distribuzione. *Inst. Ital. Atti. Giorn.* 1933; 4: 83-91.
53. Gosset WS. The probable error of a mean. *Biometrika* 1908; 6: 1-25.
54. Fisher RA. Applications of "Student's" distribution. *Metron* 1925; 5: 90-104.
55. Tan SH, Inai R, Kotaki M, Ramakrishna S. Systematic parameter study for ultrafine fiber fabrication via electrospinning process. *Polymer* 2005; 46: 6128-6134.

Received 23.10.2014 Reviewed 19.06.2015